

This is a repository copy of *Design and nonviral delivery of live attenuated vaccine to prevent chronic hepatitis C virus-like infection*.

White Rose Research Online URL for this paper:

<https://eprints.whiterose.ac.uk/id/eprint/230570/>

Version: Published Version

Article:

Trivedi, Sheetal, Dravid, Piyush, Passchier, Tim C orcid.org/0000-0002-1306-5853 et al. (11 more authors) (2025) Design and nonviral delivery of live attenuated vaccine to prevent chronic hepatitis C virus-like infection. Nature Communications. 7629. ISSN: 2041-1723

<https://doi.org/10.1038/s41467-025-62813-8>

Reuse

This article is distributed under the terms of the Creative Commons Attribution-NonCommercial-NoDerivs (CC BY-NC-ND) licence. This licence only allows you to download this work and share it with others as long as you credit the authors, but you can't change the article in any way or use it commercially. More information and the full terms of the licence here: <https://creativecommons.org/licenses/>

Takedown


If you consider content in White Rose Research Online to be in breach of UK law, please notify us by emailing eprints@whiterose.ac.uk including the URL of the record and the reason for the withdrawal request.

Design and nonviral delivery of live attenuated vaccine to prevent chronic hepatitis C virus-like infection

Received: 7 March 2025

Accepted: 31 July 2025

Published online: 15 August 2025

 Check for updates

Sheetal Trivedi^{1,7}, Piyush Dravid^{1,7}, Tim C. Passchier², Satyapramod Murthy¹, Kripa Shanker Kasudhan¹, Narendran Reguraman¹, Justin Kellar¹, Rahul Chandra¹, Cole Cassidy¹, Peter D. Burbelo³, Arash Grakoui^{4,5}, Himanshu Sharma¹, Peter Simmonds² & Amit Kapoor^{1,6} ✉

An effective vaccine for the hepatitis C virus (HCV) remains an unmet medical need. There is no animal model for assessing HCV vaccines; however, rodent hepacivirus (RHV) infection in laboratory rats recapitulates the lifelong chronic hepatotropic infection and immune evasion of HCV. Here, we designed a live-attenuated vaccine (LAV) for RHV and determined its immunogenicity and efficacy for preventing chronic infection. The LAV strains are generated by synonymous mutagenesis to increase the frequencies of naturally suppressed dinucleotides, UpA or CpG, in genomic regions that lack extensive RNA secondary structures. Rats vaccinated using LAV containing infectious virions (LAV-IV), or lipid nanoparticle-encapsulated viral RNA (LNP-vRNA) developed short-term viremia and robust T cell responses. After challenge with RHV-rn1, while all unvaccinated rats developed chronic infection, 75% and 85% of rats vaccinated with LAV-IV and LAV-vRNA cleared the infection. Clearance of RHV-rn1 was associated with expansion of memory T cells, transient rise in serum ALT, and, more importantly, enhanced protection against reinfection. In conclusion, we identified a genomic region of hepacivirus that can be synonymously mutated to attenuate its persistence, and vaccines based on these modified genomes protect against chronic hepacivirus infection, a strategy with an apparent translational path toward HCV immunization.

Since the discovery of the hepatitis C virus (HCV) in 1989¹, remarkable advances have been made in our understanding of the prevention and treatment of HCV-associated diseases². However, HCV research has failed to deliver its principal promise of developing a preventive vaccine^{3,4}. After nearly a decade of use of the highly effective HCV direct-acting antivirals that can cure most infections, it is well

understood that an effective vaccine is necessary to control the ongoing HCV transmissions and achieve the larger goal of eradication^{3–6}.

Several challenges have restricted the development of an effective HCV vaccine⁵. HCV can only naturally infect humans or chimpanzees, and thus, an immunocompetent small animal model to identify

¹Center for Vaccines and Immunity, The Research Institute at Nationwide Children's Hospital, Columbus, OH, USA. ²Nuffield Department of Medicine, University of Oxford, Oxford, UK. ³Adeno-Associated Virus Biology Section, National Institute of Dental and Craniofacial Research, National Institutes of Health, Bethesda, MD, USA. ⁴Emory National Primate Research Center, Emory University, Atlanta, GA, USA. ⁵Division of Infectious Diseases, Department of Medicine, Emory University School of Medicine, Atlanta, GA, USA. ⁶Department of Pediatrics, College of Medicine and Public Health, The Ohio State University, Columbus, OH, USA. ⁷These authors contributed equally: Sheetal Trivedi, Piyush Dravid. ✉e-mail: amit.kapoor@nationwidechildrens.org

immune correlates of protection against chronic infection and to test the efficacy of different vaccines has not been available for the past three decades since the discovery of HCV. The recent failure of a well-designed clinical trial of the HCV vaccine in humans⁷ further highlights our poor understanding of the protective immunity needed to prevent chronic infections. Another significant challenge is the extensive genetic heterogeneity of HCV variants that can be phylogenetically classified into at least 8 genotypes and over 75 subtypes^{8,9}. Genotypes differ by >30% at the nucleotide level, compared with >15% differences between subtypes. Although all major genotypes have been found worldwide, there are apparent differences in their geographical distribution¹⁰. Vaccines might therefore have to be tailored to match the genotypes prevalent in a particular population, such as genotypes 1 and 3 in most Western countries, genotypes 1, 2, 4 and 7 in sub-Saharan Africa and genotypes 1, 2 and 6 in South and Southeast Asia.

The isolation of a rodent HCV-like hepacivirus (RHV) from wild rats (*Rattus norvegicus*), RHV-rn1, was promising for the development of informative and tractable surrogate models for HCV^{11–14}. We have shown that RHV-rn1 shares genetic features and organization, poly-protein cleavage pattern, liver tropism, and DAA susceptibility with HCV, making it a relevant surrogate model for HCV^{13,15,16}. RHV-rn1 also establishes exclusively hepatotropic infection in immunocompetent inbred and outbred lab rats, and the chronic infection is also associated with immune dysfunction, resembling that of HCV infections in humans^{12,13,17}. Like HCV infection in humans and chimpanzees^{18–22}, we further demonstrated that T cell immunity plays an essential role in the clearance and control of RHV-rn1 infection in rats and mice^{12,23,24}. The subversion of T cell immunity is a critical feature of chronic, lifelong RHV-rn1 infection in inbred immunocompetent rats²⁴, and vaccination to restore virus-specific memory T cells has been shown to confer protection against chronic infection^{12,14}. Furthermore, our observations of prolonged or chronic RHV-rn1 infection in vaccinated rats after antibody-mediated depletion of CD8 or CD4 T cells and reduced vaccine efficacy against RHV-rn1 variant containing mutations in dominant MHC class I epitopes confirmed a critical role for T cells in vaccine-conferred protection^{12,17}.

Serial passaging of pathogenic viruses in vitro or in vivo to develop less pathogenic viral variants is the traditional and empirical approach of generating live attenuated vaccines (LAV). More recent approaches to achieve attenuation in a more controlled way include manipulating viral genomes using insertions and deletions, changing the natural bias for codon^{25–27}, or codon-pair usage^{28–31}, or dinucleotide frequencies^{32–35}. The latter approach achieves attenuation through increasing the frequencies of dinucleotides UpA (uracil followed by adenine) or CpG (cytosine followed by guanine), the two dinucleotides that are specifically suppressed in genomes of most vertebrate RNA viruses. While this approach was shown to substantially decrease the replication or pathogenicity of RNA viruses that cause acute resolving infections^{32,33,36,37}, it has not to date been evaluated as a mechanism to attenuate viruses associated with chronic infections.

HCV primarily causes lifelong persistent infection in 70% and liver diseases in approximately 20% of those infected. Attenuation may potentially reduce its ability to establish chronic infection, and therefore be used as LAV to induce protective immunity against chronic infection of wild-type virus. However, the development of an attenuated strain of HCV has remained problematic in the absence of efficient cell culture systems and a tractable immunocompetent animal model that reproduces the chronicity of HCV observed in humans³⁸. Notably, by transferring the developmental approach to the RHV / rat model, we were able to demonstrate how sequence-independent approaches, such as artificially increasing frequencies of naturally suppressed dinucleotides UpA and CpG, can create viable strains of RHV-rn1 with irreversible attenuation. Furthermore, these strains could be used as LAV to protect against chronic infection of the wild-type RHV-rn1. Our results showed that an in silico designed and

developed LAV for HCV-like virus, delivered through non-viral packaging in lipid nanoparticles (LNP), induced robust immunity to protect against chronic HCV-like infection.

Results

Identification of hepacivirus genomic regions that can tolerate synonymous mutations

The genomes of HCV and all vertebrate hepaciviruses characterized to date possess extensive genome-scale ordered RNA structure (GORS), a genome property associated with persistent infections that is largely absent from other members of the flavivirus family, such as the vector-borne orthoflaviviruses that primarily cause acute self-resolving infections in their mammalian hosts³⁹. Thus, we were concerned over whether the RHV genome would possess the plasticity to tolerate compositional modifications, such as artificially increased frequencies of the naturally suppressed dinucleotides, CpG and UpA, without damaging base pairing in RNA secondary structures that may be involved in in vivo replication. However, it was apparent that several regions of the RHV genome naturally showed lower degrees of RNA secondary structure, as manifested by lower mean folding energy differences (MFEDs)³⁹, from sequence order randomized controls (Fig. 1A). We hypothesized that such regions would be tolerant to the multiple synonymous mutations required to increase frequencies of UpA and CpG pairs previously associated with attenuation^{37,40}. The longest stretch of the RHV genome with lower MFED was identified in the region coding E2, p7, NS2, and the N-terminal half of the NS3 protein (R3 in Fig. 1A), with a mean MFED of 0.4% (Table S1, Supplementary Information). This contrasts with the more structured regions immediately before and after this region R2: 4.4%, R4: 4.5%). To test our hypothesis, first, we generated codon scrambled (CDLR) mutants for region R3 and the two adjacent regions on either side (R2 and R4) using the Sequence Mutate program in the SSE package³⁹ and introduced these into the previously described RHV-rn1 plasmid backbone¹³. The CDLR mutants preserve the natural nucleotide composition and dinucleotide frequencies, despite carrying hundreds of synonymous mutations (Fig. 1B)³⁷.

The full-length viral RNA transcripts of R2-CDLR, R3-CDLR, and R4-CDLR were injected into the livers of rats to initiate infection and rescue the infectious virus, as described earlier for the wild-type RHV-rn1 (Fig. 1C)¹³. The rats injected with the wild-type RHV-rn1, R2-CDLR, and R3-CDLR mutants developed viremia and remained persistently infected until observed or 175 days post-infection (pi) (Fig. 1D). Notably, the rats injected with R4-CDLR failed to be infected, with no detectable viremia or evidence for antibody seroconversion, indicating the failure of this mutant to produce viable and infectious virus. These results indicated that the R2 and R3 regions of the RHV genome can tolerate hundreds of synonymous mutations without any significant loss of virus infectivity or replication.

Nature of infection and immunity of UpA^{high} and CpG^{high} mutants

Since CDLR mutants of R2 and R3 regions were viable, we designed UpA^{high} and CpG^{high} mutants for these regions, named R2-UpA^{high}, R2-CpG^{high}, R3-UpA^{high}, and R3-CpG^{high} (Fig. 1B). After sequence confirmation of recombinant clones, their transcripts representing the complete viral genome were injected into the liver of 3 rats for each mutant. Except for the R2-CpG^{high} mutant injected rats, all others developed short-term viremia that cleared before day 21 pi (Fig. 1E). Interestingly, all rats infected with RHV-rn1, R2-CDLR and R3-CDLR mutant seroconverted as evident from the rise of high-titers of anti-NS3 IgG antibodies in their serial serum samples (Fig. 2A), but the rats infected with R2-UpA^{high}, R3-UpA^{high}, and R3-CpG^{high} despite short-term viremia, did not develop high-titers of anti-NS3 IgG antibodies. Notably, RHV-rn1, R2-CDLR, R3-CDLR, and R4-CDLR rats showed a complete absence of functional virus-specific T cell responses, as evident from the lack of IFN- γ producing T cells in their PBMC samples stimulated with RHV T cell epitopes (Fig. 2B). These results indicated that the

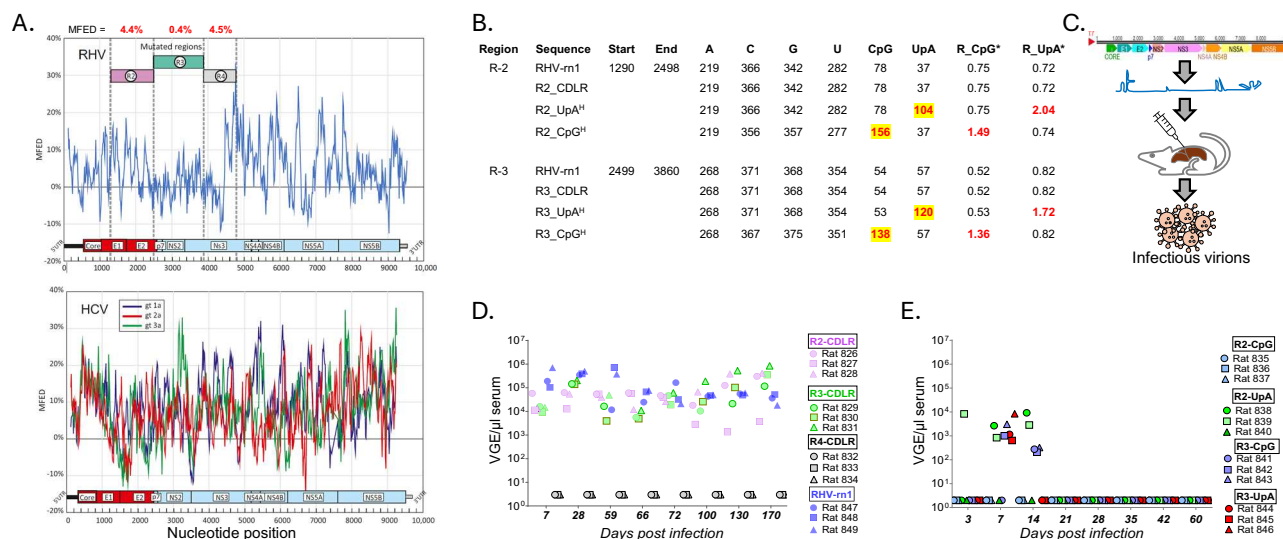


Fig. 1 | Design of RHV mutants evaluated as LAV vaccine candidates and their infection outcomes in rats. **A** The minimum folding energy differences (MFED) in the RHV-rn1 genome were plotted as the blue line in the upper panel and for different HCV genotypes in the lower panel. MFED values were calculated for consecutive 240 base fragments, incrementing by 15 bases across the genome. MFED values were calculated by subtraction of the MFE of the native sequence from the mean value of the same sequence scrambled in base order while maintaining native dinucleotide frequencies. R2-4 depicts the genomic regions selected for mutagenesis, and their MFED values are shown in red fonts. **B** Table shows mononucleotide and dinucleotide compositions of wild-type (RHV-rn1), CDLR, and UpA- and CpG-maximized sequences in R-2 and R-3 regions. The yellow highlighted

numbers indicate the final number of dinucleotides in the R-2 and R-3 regions of the UpA and CpG mutants. *Ratio of observed frequencies of CpG or UpA frequencies to expected values based on mononucleotide composition. **C** Schematics of in vivo rescue of infectious virus from mutated genomes using intrahepatic injection of transcribed RNA in rats. Each rat was injected with 10 µg viral RNA in PBS. **D** Course of viremia of CDLR mutants and wild-type RHV-rn1. Note that the CDLR-4 mutant failed to produce consistent and high-titer viremia observed in R2 and R-3 CDLR mutants. **E** Course of viremia in rats injected with R-2 and R-3 variants with elevated UpA or CpG dinucleotide frequencies. Source data are provided as a Source Data file.

chronic infection with CDLR mutants was associated with the same dysfunctional T cell immunity as observed on infection with the wild-type RHV-rn1, as observed in our earlier studies^{12,16}. Importantly, the rats injected with three mutants, R2-UpA^{high}, R3-UpA^{high}, and R3-CpG^{high} developed antigen-specific IFN-γ producing T cells that were enumerated by analyzing their peripheral blood mononuclear cells (PBMC) (Fig. 2B), and the highest and the most consistent antigen-specific T cell responses were present in the R3-UpA^{high} injected rats (Fig. 2B–C). These results indicate that the self-resolving infection of R2-UpA^{high}, R3-UpA^{high}, and R3-CpG^{high} mutants generated virus-specific memory T cells that could produce antiviral cytokines upon antigenic stimulation.

To determine if the spontaneous clearance of R3-UpA^{high} and CpG^{high} mutants conferred protection against chronic infection, we challenged these mutant-cleared (or vaccinated) rats with 10⁵ VGE of wild-type RHV-rn1 virus, which is equivalent to >10-fold the minimum infectious dose to establish chronic infections in rats. All three R2-CpG^{high} vaccinated rats developed a chronic infection (Fig. 2E), whereas only one of the three rats vaccinated with R2-UpA^{high} mutant developed a chronic infection. Similarly, all three R3-CpG^{high} vaccinated rats developed acute viremia, but only one remained persistently viremic. Notably, all three R3-UpA^{high} mutant vaccinated rats developed acute viremia then cleared the RHV-rn1 infection within two weeks (Fig. 2F). Altogether, these results indicated that the spontaneous clearance of R3-UpA^{high} mutant conferred the most efficacious protection against the chronic infection of the homologous wild-type virus, RHV-rn1, which universally produces lifelong HCV-like chronic infection in unvaccinated rats^{12,13,16,17}. Although both R3-UpA^{high} and R3-CpG^{high} mutants induced equivalent T cell responses (Fig. 2B), considering the results of protection studies (Fig. 2F), we focused all subsequent experiments on the R3-UpA^{high} mutant. However, to generate the R3-UpA^{high} mutant virus stock sufficient for vaccination, we injected transcripts of the R3-UpA^{high} clone into the livers of Lewis rats that were

transiently depleted for CD4 T cells since the infection in normal Lewis rats was yielding low titers of viremia (Fig. 2F). The serum of two CD4 T cell-depleted Lewis rats euthanized on day 7 pi was pooled and used in all subsequent studies as the live attenuated vaccine containing infectious virions, LAV-IV.

LAV-IV induced robust liver-resident T cell immunity in rats and mice

Rats infected with 10⁵ VGE of serum-derived R3-UpA^{high} virus developed 1–2 weeks of viremia that was significantly lower in titers than viremia observed after RHV-rn1 infection (Fig. 3A). Infected rats variably seroconverted and developed virus-specific T cell responses against multiple viral proteins (Fig. 3B, C). To further characterize R3-UpA^{high} induced T cell immunity in rats, we used peptide pools representing the complete RHV polyprotein, a peptide pool representing previously identified CD8 and CD4 T cell epitopes, and rat MHC class I tetramers specific to peptides from E1 and NS5B proteins, as described earlier^{12,16,17}. The virus-specific memory T cells were more frequent in the liver than the spleen and predominantly targeted the nonstructural proteins, as reported during RHV and HCV infection^{41,42}. The frequencies of MHC class I tetramers-specific CD8 T cells ranged from 2–7% of total CD8 T cells in the liver in vaccinated rats (Fig. 3D). Notably, compared to the total CD8 T cells in the liver, almost all vaccine-specific CD8 T cells expressed chemokine receptor CXCR3 and were negative for expression of L-selectin CD62L indicating that these cells were recruited to the liver and represent the effector tissue-resident memory (T_{RM}) CD8 T cells (Fig. 3E).

For a more thorough characterization of R3-UpA^{high} induced T cell immunity, we used laboratory mice. Notably, unlike in rats, the infection of RHV-rn1 spontaneously resolves within weeks in normal laboratory mice⁴¹. Thus, although lab mice are not meaningful models for assessing vaccine efficacy against chronic infection, the recently generated RHV-specific mouse MHC class I and class II tetramers⁴¹,

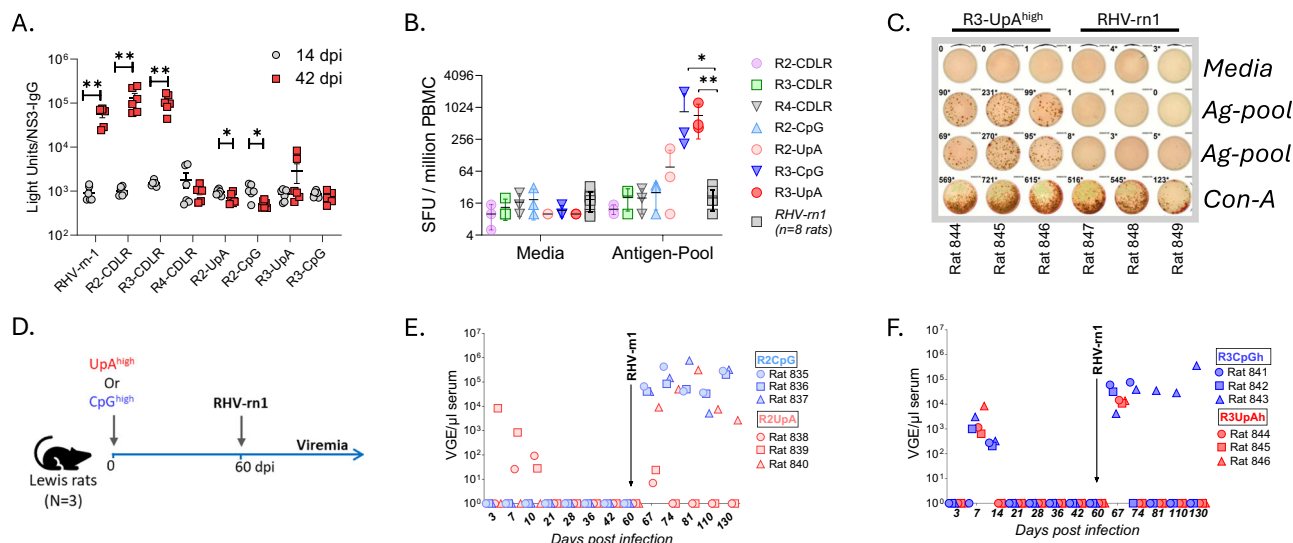


Fig. 2 | Nature of immunity and protection conferred by RHV-rn1 and mutant viruses. **A** Anti-NS3 IgG titers in the serum of rats infected with RHV-rn1 and different mutants ($n = 6$). Data are presented as individual values and mean \pm SEM. Two-tailed paired t-test was used for analysis, and p -values < 0.01 or 0.05 were considered statistically significant; p -values between day14 and day42 for RHV-rn1 (**, 0.002), R2-CDLR (**, 0.01), R3-CDLR (**, 0.002), R2-UpA (*, 0.034), and R2-CpG (*, 0.035). Sequences of R2 and R3 regions of RHV-rn1 and mutants are available as Supplementary Information S3. **B** Spot forming units (SFU) indicating the IFN- γ secreting T cells in ELISPOT assay in PBMC stimulated with a pool of peptides

representing the RHV-rn1 T cell epitopes. PBMC were collected on 28–31 dpi. SFU in the antigen pool of mutants was compared to RHV-rn1 ($n = 8$ rats) using a two-tailed unpaired t-test, and p -values for R3-CpG (*, 0.0285) and R3-UpA (**, 0.001) as compared to RHV-rn1 in Antigen-Pool. Data points are presented as individual values and error bar at mean \pm SD. **C** Image of ELISPOT assay showing the SFU counts in rats infected with R3-UpA^{high} and RHV-rn1 at 28 dpi. **D** Outline of vaccination and challenge studies. **E, F** Rats that cleared the R-2 and R-3 mutants were challenged with wild-type RHV-rn1 and followed for viremia for > 2 months post-infection. Source data are provided as a Source Data file.

together with the availability of a vast array of antibodies for mouse immune cell markers, make them a valuable model for characterizing RHV-specific T cells. The R3-UpA^{high} produced self-resolving infection in mice. Additionally, the acute viremia in R3-UpA^{high} mice was lower in titers than in RHV-rn1 viremia in mice, indicating that higher frequencies of UpA also attenuated the RHV ability to establish high-titer and extended viremia in mice (Fig. 3F). We used mouse MHC class I (*H2-D^b*) and class II (*H-2A^b* or *I-A^b*) tetramers to compare the RHV NS3-specific memory CD8 and CD4 T cells in R3-UpA^{high} and RHV-rn1 cleared mice. The frequencies of antigen-specific memory CD8 T cells in R3-UpA^{high} mice were significantly lower in both the liver and spleen compared to those in RHV-rn1 mice, possibly due to the higher and prolonged viremia in the latter. However, there were no differences in the antigen-specific memory CD4 T cell frequencies between the groups (Fig. 3G). The antigen-specific memory CD8 T cells in the liver (tissue-resident memory, T_{RM}) of both RHV-rn1 and R3-UpA^{high} were remarkably different from their homologs in the spleen, specifically in the expression of CD62L, CD69, LFA-1, SLAMF7, and CD127 (Fig. 3H). Similar differences were not found between the antigen-specific memory CD4 T cells (Fig. 3I). Notably, the median fluorescence intensity of PD-1 was higher on antigen-specific memory CD8 T cells in the RHV-rn1 mice compared to the R3-UpA^{high} mice in both spleen and liver, likely due to the more prolonged exposure of T cells to antigen in RHV-rn1 mice (Fig. 3H). Overall, these results confirmed that R3-UpA^{high} clearance generates robust memory CD8 and CD4 T cells that largely resemble the liver-resident nature of memory T cells generated by natural clearance of wild-type RHV-rn1 virus.

LAV-IV vaccination conferred protection against chronic infection

A total of 24 rats, 12 males and 12 females, were infected with the R3-UpA^{high} virus as the prime and booster doses for LAV-IV vaccination (Fig. 4C). A short-term viremia was observed in most rats after the prime and booster doses, but one rat (rat-726) developed chronic infection after the prime dose and remained viremic throughout the

follow-up period (Fig. 4C). Notably, the viremia on day 7 pi in males was significantly higher in titers than in the females after the prime dose (Fig. 4D). The remaining 23 rats that cleared the vaccine were challenged with 10^5 VGE of RHV-rn1. The RHV-rn1 challenge inoculum was the serum of an infected Lewis rat, as described earlier^{12,17}. Notably, the Lewis rats infected with RHV-rn1, regardless of age or sex, universally develop lifelong chronic infections accompanied by high titers of viremia^{12,13,16,17,43,44}. Of the 23 LAV-IV vaccinated rats, 21 developed viremia after the challenge infection, and importantly, 17 of 23 rats cleared the viremia within 4 weeks and remained cleared until observed or day 100 post-challenge. An additional vaccinated rat cleared the viremia in two months; thus, by the end of the study, 18 of 23 vaccinated rats cleared the infection, indicating $> 75\%$ efficacy of the LAV-IV vaccine in preventing chronic infection (Fig. 4C). Challenge infection was associated with robust expansion of virus-specific T cells with specificities to RHV structural and nonstructural proteins (Fig. 4E). Interestingly, the rats that developed chronic infection had significantly higher titers of viremia on day 7 after challenge infection compared to the cleared rats indicating that the vaccine failure was associated with poor control of viremia during the acute phase infection, more likely indicating the lack of robust vaccine-induced immunity in these rats (Fig. 4F). Comparison of virus-specific T cells frequencies in 6 vaccinated rats before and after challenge also showed significantly lower expansion of vaccine-induced T cells in the rats that developed chronic infection (Fig. 4G). Terminal analysis of virus-specific T cells in the liver of cleared and chronic rats showed that the persistent viremia was associated with exhaustion of T cell antiviral functions (Fig. 4H), and the virus-specific CD8 T cells in cleared and chronic rats differed in their phenotype, specifically in the expression of CXCR3 and CD161 (Fig. 4I).

To determine if the chronic R3-UpA^{high} infection in rat-726 was due to the reversion of UpA mutations, we sequenced the complete genome of the virus in serum on days 14 and 165 pi. On day 14 pi, the virus genome had all 160 synonymous mutations introduced to increase the UpA frequencies and only one new synonymous mutation at position

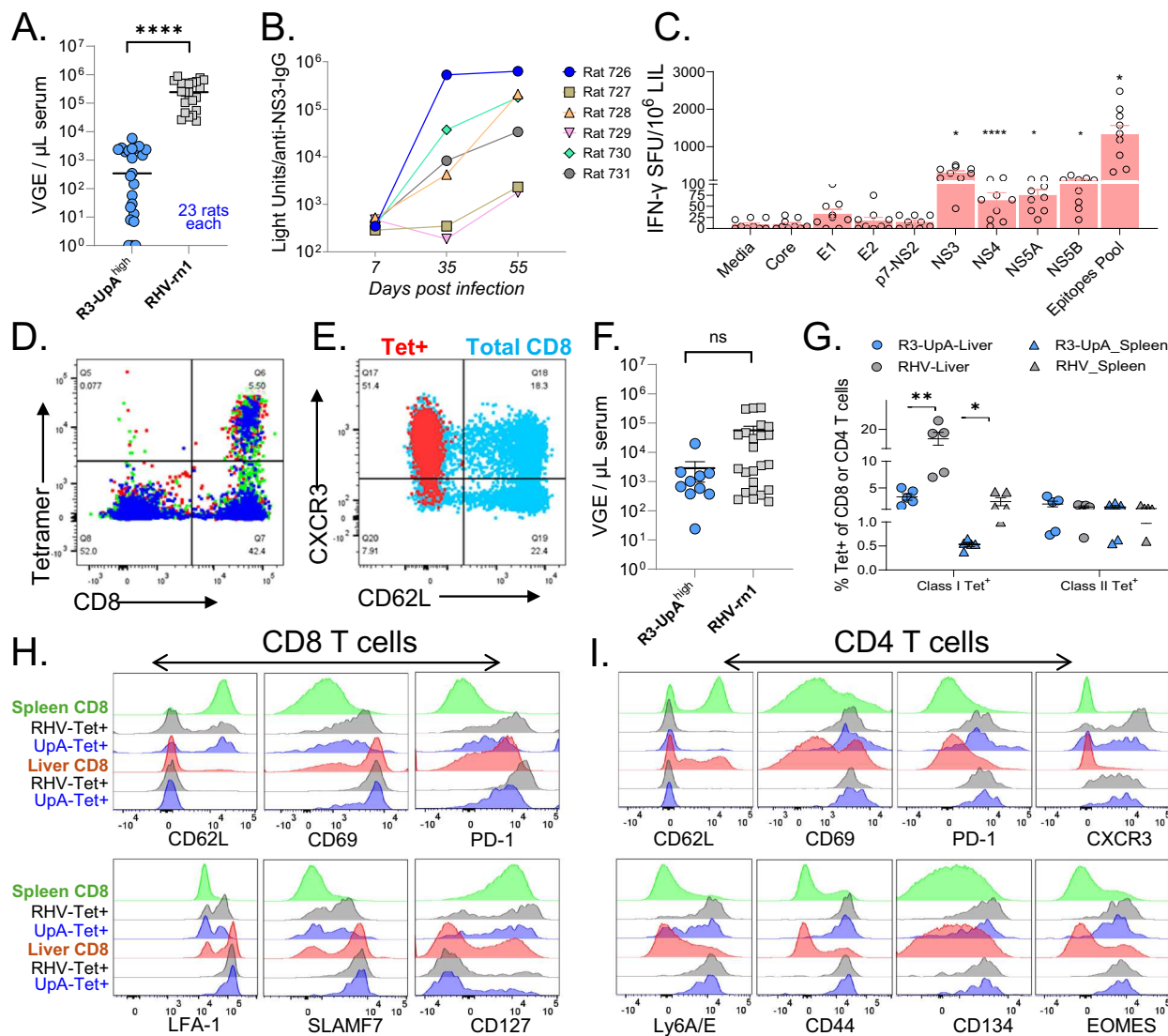


Fig. 3 | Nature of viremia, antibody and antigen-specific T cells induced by R3-UpA mutant in rats and mice. A Viremia in R3-UpA^{high} and RHV-rn1 infected rats (23 rats in each group) on 7 dpi. RHV-rn1 viremia data were compiled from our other studies using the same viral stock and from 8 rats used as controls in this study. Two-sided unpaired t-test was performed; p -value (****, <0.0001). **B** Serum anti-NS3 IgG antibody titers after R3-UpA^{high} infection in six vaccinated rats. **C** Specificities of antigen-specific T cells isolated from the liver of R3-UpA^{high} infected rats ($n = 3$) at 14 dpi, three animals with their 3 replicates were shown as dots. Unpaired t-test and p -values between Media and NS3 (*, 0.0269), NS4 (***, 0.0006), NS5A (*, 0.0403), NS5B (*, 0.0429), Epitopes-Pool (*, 0.0358) respectively. Data points are presented as individual values and error bar at mean \pm SEM. **D** Rat MHC class I tetramer incorporating an NS5B peptide was used to determine the frequencies of virus-specific CD8 T cells in the livers of R3-UpA vaccinated rats euthanized on 14 dpi. Representative data from three rats were shown using different colors.

E Representative data showing the difference in phenotype of vaccine-primed memory CD8 T cells specific for NS5B peptide (red) and total CD8 (blue) T cells in the liver of vaccinated rats. **F** Viremia in R3-UpA^{high} ($n = 10$) and RHV-rn1 infected mice on day 7 pi. Two-tailed unpaired t-test with p -value = (ns, 0.1222). Data points were shown with mean \pm SEM. **G** Frequencies of mouse MHC class I and class II specific CD8 and CD4 T cells in the liver (circle) and spleen (triangle) in R3-UpA and RHV-rn1 cleared mice ($n = 5$) on 45 dpi. Two-tailed unpaired t-test for Class I Tet⁺ response between R3-UpA Liver and RHV-Liver (**, 0.0084) and between R3-UpA Spleen and RHV-Spleen (*, 0.0356). Data points are presented as individual values and error bars at mean \pm SEM. **H** Comparative analysis of total CD8 T cells in the liver and spleen with antigen-specific memory CD8 T cells in R3-UpA and RHV mice on 45 dpi. **I** Comparative analysis of total CD4 T cells in the liver and spleen with antigen-specific memory CD4 T cells in R3-UpA and RHV mice on 45 dpi. **H** and **I** use the same color scheme. Source data are provided as a Source Data file.

3465. Interestingly, the virus genome from 165 dpi serum showed reversions of 9 introduced UpA sites and 4 new synonymous mutations that disrupted naturally occurring UpA sites. Additionally, 19 new synonymous and 22 new non-synonymous mutations were also present, mainly in E1E2 and NS5A proteins (Fig. 4J). The extent of virus evolution in rat-726 was greater than that observed during chronic RHV-rn1 infection in naïve or vaccinated rats, or during chronic infection in immunocompromised mice^{12,13,17,43–45}. We infected three naïve rats with the rat-726 day 165 pi serum, and all rats developed a chronic infection, indicating the complete reversion of LAV attenuation in rat-726 during the chronic infection.

Nonviral delivery of R3-UpA genomes as lipid nanoparticles produced viremia and immunity against chronic infection

We realized two limitations of the LAV-IV studies that would be of relevance for future translation to HCV vaccines. First, although an R3-UpA^{high} version of HCV can be designed and synthesized, the in vitro systems for HCV may not be robust enough to rescue sufficiently high-titer mutated virus stocks. For RHV, this problem was circumvented by producing vaccine stocks in Lewis rats that were transiently depleted for CD4 T cells. Second, the in vitro or in vivo propagation of attenuated viruses inherently increases the risk of reversion of introduced mutations (Fig. 4I). Thus, we aimed to determine if lipid nanoparticle (LNP)

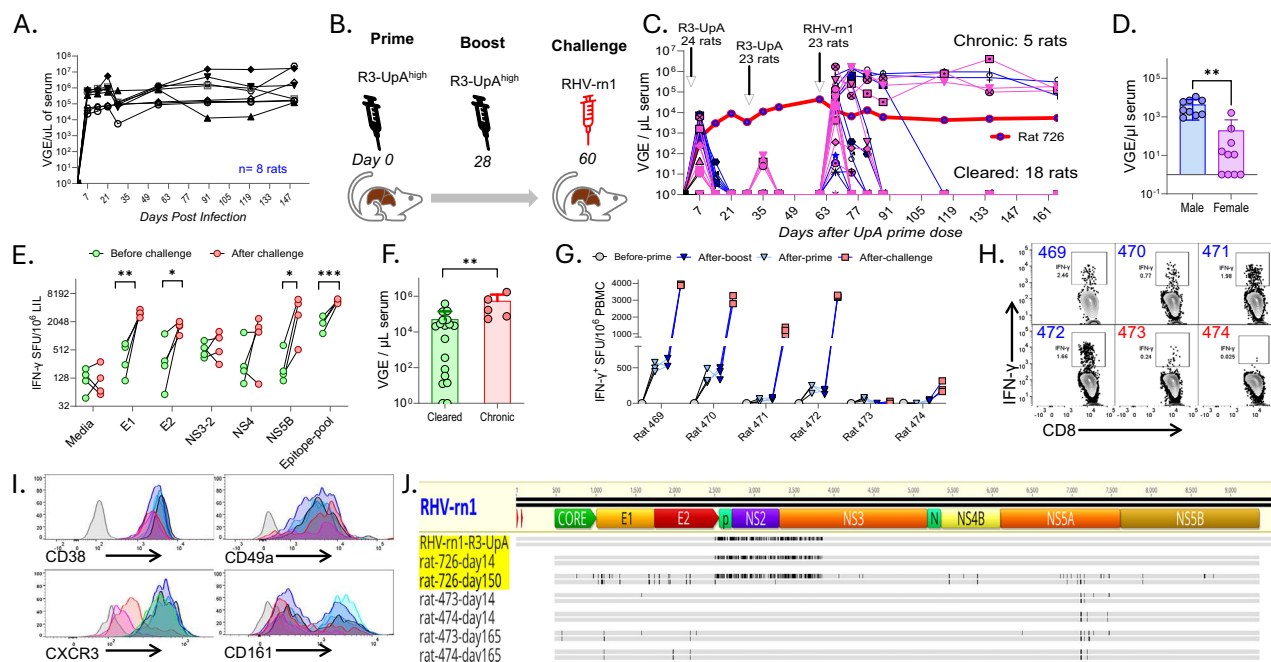


Fig. 4 | Infection, immunity, and protection of LAV-IV vaccine. **A** Course of viremia in 8 RHSV-m1 infected naïve rats. **B** Experimental outline and timeline of vaccination and challenge study. **C** Course of viremia after R3-UpA^{high} prime and booster vaccination and RHSV-m1 challenge infection in 12 male (blue) and 12 female (pink) rats. In vivo rescued R3-UpA^{high} virus was used for vaccination. Rat-726 (male) developed persistent viremia of the R3-UpA virus, shown as a blue circle and red connecting lines. **D** Comparison of R3-UpA viremia after prime dose in male ($n = 9$) and female ($n = 10$) rats at day 7 pi. Two-tailed unpaired t-test between Male and Female group, p -value = (**, 0.0024). Data points are presented as individual values and error bars at mean \pm SD. **E** Comparison of virus-specific T cell frequencies targeting different viral proteins before and after 14 days of RHSV-m1 challenge in 4 vaccinated rats. The frequencies of IFN- γ secreting T cells, shown as SFU, in ELISPOT assay in LILs stimulated with a pool of peptides representing the RHSV-m1 T cell epitopes. The mean value of SFU counts in triplicate wells is shown. Two-tailed paired t-test- before and after challenge for each peptide pool. P -values for E1 (**, 0.006), E2 (*, 0.0106), NSSB (*, 0.036) and Epitope-Pool (***, 0.0001). **F** Viremia on day 7 after RHSV-m1 challenge in rats that subsequently cleared the infection

($n = 18$) or remained chronic ($n = 5$). Two-tailed unpaired t-test; p -value (**, 0.0066). Data points are presented as individual values and error bars at mean \pm SD. **G** Frequencies of virus-specific IFN- γ + T cells in PBMC of rats, before and after RHSV-m1 challenge, showing their significant expansion after challenge, on 9 dpi. Rat 473 and 474 developed chronic RHSV-m1 infection. **H** Frequencies of CD8 T cells producing IFN- γ after antigen stimulation in the liver of cleared (blue font) and chronic (red font) rats after 100 dpi. **I** Surface expression of various CD8 T cell markers shown as Fluorescence minus one (FMO) control (grey) and rat MHC class I Tetramer+ CD8 T cells in the liver of cleared (shades of blue) and chronic (shades of red) rats. **J** Sequence alignments of RHSV-m1 and R3-UpA genomes recovered from rats that developed chronic infection. The parallel grey lines show nucleotide (upper) and amino acid (lower) mutations (black marks) compared to the RHSV-m1 genome. Alignment was generated using a consensus sequence derived from >200 X coverage of each nucleotide position, and the recognized base was present in >75% of sequence reads. The sequences are submitted to GenBank (PV639513-PV639519). Source data are provided as a Source Data file.

technology can be used to encapsulate R3-UpA^{high} genomes and if these viral-RNA (vRNA) LNP complexes can initiate infection for immunization. Since the R3-UpA^{high} virus produced lower titer and shorter viremia, as proof-of-principle, we first made vRNA-LNP using full-length transcripts of RHSV-m1 genome, and all 3 rats injected intravenously with 5 μ g of encapsulated RNA developed high-titer viremia that persisted throughout the 120-day follow-up period. Then, we vaccinated 12 male and 12 female rats, with two doses of R3-UpA^{high} vRNA-LNP; each dose used 5 μ g of LNP encapsulated vRNA (Fig. 5A). We observed short-term viremia after the prime and booster dose, and all 24 vaccinated rats cleared the viremia (Fig. 5B). The vaccinated rats were challenged with 10^5 VGE of RHSV-m1, which represents >10-fold the minimum infectious dose. Of the 24 rats, 21 cleared the RHSV-m1 infection within 4 weeks, indicating a vaccine efficacy of >85% against chronic infection. Of the three chronic rats, two were females and one was male.

To determine the relative importance of vaccine-elicited CD4 versus CD8 T cells in protection against chronic RHSV-m1 infection, vRNA-LNP vaccinated rats were treated with depleting antibodies targeting these subsets immediately prior to RHSV-m1 challenge. While all control rats cleared the RHSV-m1 infection, both CD4 and CD8-depleted rats failed to clear or control the virus and remained viremic until observed (Fig. 5C). These results indicate that the vRNA-LAV conferred protection was dependent on the presence of both CD8 and CD4 T cell subsets.

Furthermore, consistent with T cells being primary mediators of vaccine-conferred protection, the control of RHSV-m1 viremia was associated with a significant rise in serum alanine aminotransferase enzyme levels that normalized with the clearance of viremia (Fig. 5D). Although the mean of peak ALT values after the challenge was 94.5 IU/L, indicating only mild to moderate liver pathologies⁴⁶.

To study the T cell immunity after vaccination and challenge, we enumerated the virus-specific T cells in serially collected PBMC samples using ELISPOT assay and two MHC class I tetramers specific for epitopes in E1 and NSSB proteins. Although the difference between the frequencies of the IFN- γ -producing vaccine-specific T cells in rats that cleared or developed chronic RHSV-m1 infection was not statistically significant, expansion of IFN- γ -producing antigen-specific T cells after challenge was observed in only one of three chronic rats (Fig. 5E). Additionally, the expansion of both NSSB- and E1-specific CD8 T cells was relatively less in the chronic rats compared to the cleared rats during the early as well as late phases of challenge infection (Fig. 5F, G). Analysis of virus-specific T cell antiviral functions in the liver at terminal time points revealed that the chronic infection with the challenge virus was associated with the exhaustion of virus-specific CD8 T cell function (Fig. 5H).

Finally, to determine the nature of protective immunity and whether the clearance of the challenge infection in vRNA-LNP

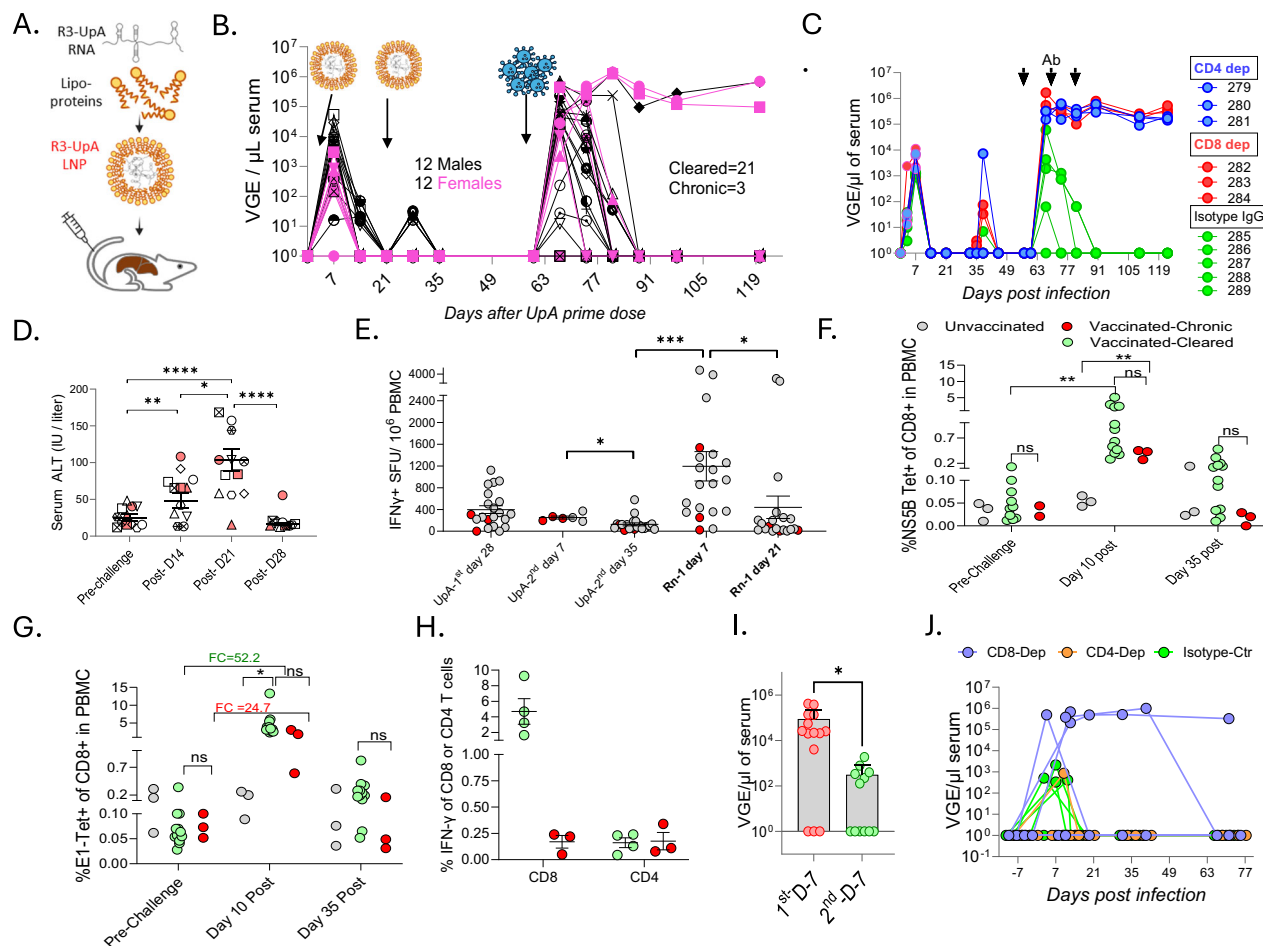


Fig. 5 | Infection, immunity, and protection of LNP-vRNA vaccine.

A Composition of R3-UpA vRNA-LNP vaccine. **B** Timeline of vaccination and challenge studies, and course of viremia in vaccinated rats. **C** Vaccinated rats were transiently depleted for CD8 α ($n=3$) or CD4 ($n=3$) T cells by antibody (Ab) or isotype control ($n=5$) before challenge with RHV-rn1 to assess the role of T cell subsets in vaccine-induced immunity. **D** Serial analysis of serum ALT values in 12 vaccinated rats before and after RHV-rn1 challenge. Rats that developed chronic infection are shown in red-filled shapes. Two-tailed unpaired t-test and p -value for Pre-Challenge vs Post-D14 (**, 0.0047), Pre-Challenge vs Post-D21 (****, <0.0001), Post-D14 vs Post-D21 (*, 0.0242) and Post-D21 vs Post-D28 (****, <0.0001). Data points are presented as individual values and error bars at mean \pm SEM. **E** Serial analysis of virus-specific T cells in PBMC of rats using IFN- γ ELISPOT assay. The frequencies of IFN- γ secreting T cells, shown as SFU, in ELISPOT assay in LILs stimulated with a pool of peptides representing the RHV T cell epitopes. The mean value of SFU counts in triplicate wells is shown. The number of animals whose PBMC samples were available for analysis is shown in parentheses; UpA 1st day28 ($n=21$), UpA 2nd day7 ($n=6$), UpA 2nd day35 ($n=21$), Rn-1 day7 ($n=20$), and Rn-1 day21 ($n=20$). Two-tailed unpaired t-test and p -value between UpA 2nd day7 vs UpA 2nd day35 (*, 0.0284); UpA-2nd day35 vs Rn-1 day7 (***, 0.0006); Rn-1 day7 vs Rn-1 day21 (*, 0.0327). **F, G** Serial analysis of the frequencies of NS5B_{251L}- and E1_{191L}-specific CD8 T cells in the PBMC of unvaccinated (grey) and vaccinated rats that

cleared (green) or developed chronic the RHV-rn1 challenge infection (red). FC=folds change. Two-tailed unpaired t-test and p -values between pre-challenge and day 10 post for cleared (**, 0.0081); and between unvaccinated and chronic (**, 0.0046). In Fig. 5F, p -values for Pre-challenge, Day 10 post, and Day 35 post (cleared vs chronic) were ns (0.5562, 0.8372, and 0.1492, respectively). In Fig. 5G p -values for Pre-challenge, Day 10 post, and Day 35 post (cleared vs chronic) were ns (0.8372, 0.1740, and 0.1581, respectively). **H** Frequencies of cells producing IFN- γ in intracellular cytokine production assay (ICS) of liver infiltrating leukocytes isolated from vaccinated rats with cleared ($n=4$, green) and chronic ($n=3$, red) RHV-rn1 infection. For ICS, cells were stimulated for 5-h with pools of peptides representing RHV T cell epitopes at 10 μ g/mL concentration. Data points are presented as individual values and error bars at mean \pm SEM. P -values for % IFN- γ of CD8 and CD4 between cleared and chronic were ns (0.0665, 0.8703, respectively). **I** Viremia titers on day 7 after the first ($n=14$) and second ($n=12$) RHV-rn1 challenge infection. Two-tailed unpaired t-test was performed, and a significant p -value was shown as * (0.0371). Data points are presented as individual values and error bars at mean \pm SD. **J** Protective immunity against reinfection in rats that cleared the primary RHV-rn1 challenge infection. Viremia after RHV-rn1 reinfection in IgG-isotype control (green, $n=7$), anti-CD8 α (blue, $n=4$), and anti-CD4 (brown, $n=4$) cell-depletion antibody-treated rats. Source data are provided as a Source Data file.

vaccinated rats enhanced protective immunity, we re-infected the cleared rats with 2×10^5 VGE of RHV-rn1. The titers of viremia after the second RHV-rn1 infection were significantly lower than those after the first infection (Fig. 5I), and all rats cleared the viremia by day 14 pi. Finally, three groups of 4 RHV-rn1 cleared rats were given CD4 or CD8 T cell depletion antibody or matching isotype antibody 3 days before RHV-rn1 reinfection (Fig. 5J). The isotype antibody-injected rats did not develop viremia, indicating very efficient control of the reinfection; only one CD4 T cell-depleted rat showed short-term viremia, while 3 of 4 CD8 T cell-depleted rats developed viremia, and one of these

rats remained chronically infected until observed, day 70 post-reinfection. These results indicated that the protection observed against chronic infection in these vaccinated and RHV-rn1-cleared rats largely depended on the presence of memory CD8 T cells.

Discussion

HCV is unique among RNA viruses in its ability to suppress and evade host immunity, thereby establishing a lifelong, persistent infection in most infected individuals. Despite being one of the most researched viruses, the mechanisms underlying immune subversion, or the

determinants of protective immunity, remain poorly understood, primarily due to the lack of a meaningful animal model³⁸. Thus, the shared genetic origin of RHV, strict hepatotropism, and its ability to subvert immunity to establish lifelong persistent infection in immunocompetent lab rats make it a meaningful model to test the design and effectiveness of HCV vaccines⁴. Although HCV genotypes are remarkably diverse in their polyprotein sequences, RHV polyprotein is even more divergent¹³. Thus, we focused on using a protein sequence-independent approach to develop the RHV vaccine, thereby increasing the translational relevance of this work for HCV vaccine development.

Our earlier work showed that the structural proteins encoding region of HCV contains fewer RNA secondary structures and has lower MFED values⁴⁷. We analyzed the RHV genome and observed a similar pattern of MFED non-uniformity across the genome (Fig. 1A). We expected these lower-MFED regions to be tolerant to large numbers of synonymous mutations that allow substantial increases in frequencies of the naturally surpassed dinucleotide pairs, UpA and CpG. To demonstrate that the observed attenuation resulted directly from the introduction of UpA and CpG dinucleotides instead though an unintended effect on RNA secondary folding or the disruption of uncharacterized *cis*-replication elements or cryptic alternative open reading frames, we first generated CDLR mutants³⁷, which, despite also containing a comparable number of synonymous mutations, preserve the nucleotide composition and, importantly, the native frequencies of all dinucleotides (Fig. 1B). The observation that CDLR mutants in the R-2 and R-3 regions showed a WT phenotype discounts these alternative explanations for the attenuation of the R2 and R3 CpG^{high} and UpA^{high} mutants. The non-viability of the R4 mutants may have originated from the disruption of an area of RNA structure required for replication in the NS3 protein region, coinciding with the marked spike in MFED values in this region (Fig. 1). We observed that both UpA and CpG high mutants produced equivalent viremia and acute self-resolving infection, but since our goal was also to generate robust immunity, considering that the more uniform and higher magnitude of T cell responses observed in R3-UpA^{high} cleared rats, we pursued all subsequent studies of immunity and vaccination on this mutant (Fig. 2). Additionally, the selection of R3-UpA^{high} was appropriate since R2-UpA^{high}, R2-CpG^{high}, and R3-CpG^{high} cleared rats remained partially susceptible to chronic RHV-rn1 infection upon challenge. However, we acknowledge that the initial studies of the intrahepatic injection of RNA to rescue viruses were done in a limited number of rats.

Intrahepatic injection of R3-UpA^{high} genomic RNA yielded a very low-titer and transient viremia that was insufficient to generate a vaccine stock for detailed analysis of immunogenicity and protection. Thus, first, we injected the low-titer serum in two immunodeficient SRG rats (Sprague Dawley, Rag2^{-/-}, Il2rg^{-/-}), and both rats developed robust viremia that persisted until observed day 60 pi, indicating that adaptive immune responses are necessary for the control and clearance of R3-UpA^{high} infection. Since the inherent immunodeficiency of these rats and prolonged replication of R3-UpA^{high} might have favored the reversion of attenuating mutations, we decided to use rats with transient CD4 T cell depletion to generate the LAV-IV stock. The rats were treated with CD4 T cell-depleting antibodies before R3-UpA^{high} infection and were euthanized on day 7 to collect all serum for making LAV-IV vaccine stock.

A detailed characterization of immunity in R3-UpA^{high} cleared rats was essential to understand the mechanism and immune correlates of protection against chronic RHV-rn1 infection (Fig. 3). We observed that rats infected with serum-derived R3-UpA^{high} vaccine developed variable levels of anti-NS3 IgG and T cell responses, as expected since the duration and levels of viremia were also variable among rats. However, the slight differences in viremia, its short duration, and immunological data from a fraction of rats precluded correlation analysis. Additionally, the quantity of serially collected serum samples was limited,

making simultaneous analysis of low-titer viremia and serology challenging. However, we analyzed six rats for anti-NS3 IgG levels, and of the two with the lowest IgG titers after the booster dose, one cleared, while the other developed a chronic infection upon RHV-rn1 challenge, indicating a lack of a strong correlation between the anti-NS3 IgG titers before challenge and the infection outcomes. The R3-UpA^{high} cleared rats developed liver-resident memory T cells specific to multiple viral proteins, and as observed earlier for RHV and HCV, the T cell responses predominantly targeted the nonstructural proteins (Fig. 2)⁴². Although the lack of rat-specific antibodies for many T cell markers and MHC class II tetramers precluded detailed analysis of virus-specific T cell phenotype and functions in vaccinated rats, we determined that the vaccine-induced liver-resident CD8 T cells resembled the CD8 T_{RM} cells since they were negative for CD62L expression and positive for CXCR3, contrasting with most CD8 T cells infiltrating the liver.

For more detailed characterization of R3-UpA^{high} induced T cells, we used the mouse model and the recently developed tetramers⁴¹ and, more importantly, compared the nature of R3-UpA^{high} induced T cells with those present in the wild-type RHV-cleared mice (Fig. 3). The R3-UpA^{high} mice had lower frequencies of antigen-specific memory CD8 T cells. It is plausible that the lower titers of viremia in R3-UpA^{high} mice required lower expansion of CD8 T cells to clear the virus, leading to fewer memory CD8 T cells than those in the RHV-rn1-infected mice. The direct visualization of vaccine-specific CD4 T cells in R3-UpA^{high} mice confirmed their existence and allowed their phenotypic characterization. Comparison of the phenotypes of R3-UpA^{high} and RHV-rn1 induced T cell subsets with those of total T cell subsets in the spleen and liver revealed stark differences in virus-specific central memory T (T_{CM}) cells in the spleen and T_{RM} cells in the liver. As described earlier and in other models of viral infections, virus-specific CD8 T_{RM} cells were CD62L negative and expressed higher levels of CD69 and LFA-1 compared to the virus-specific CD8 T_{CM} cells (Fig. 3H)^{41,48}. Almost all virus-specific CD8 T_{RM} cells also expressed higher levels of SLAMF7, indicating their highly cytotoxic nature and the capability to produce large amounts of cytolytic molecules, such as perforin and granzymes, upon antigen encounter⁴⁹. Notably, the virus-specific CD8 T_{RM} cells in R3-UpA^{high} mice expressed lower levels of PD-1 compared to RHV-rn1 cleared mice, possibly because the effector CD8 T cells in RHV-rn1 mice were exposed to higher levels of antigen and for a longer duration. It remains to be determined whether RHV-rn1 or R3-UpA primed CD8 T_{RM} cells will differ in their anamnestic responses during the *in vivo* challenge, as the mouse model is not susceptible to RHV chronic infection. A smaller fraction of virus-specific CD8 T_{RM} cells compared to the T_{CM} cells were positive for CD127, the receptor for interleukin-7 and a marker of long-lived memory T cells crucial for long-term immune protection against pathogens. Interestingly, the virus-specific CD4 cells were also distinct in their phenotype compared to the total CD4 T cells in the liver and spleen; however, no apparent differences were observed between virus-specific CD4 T_{RM} and T_{CM} cells in R3-UpA or RHV-rn1 cleared mice (Fig. 3I).

Considering the uneven and very short viremia observed in R3-UpA^{high} rats, we used two doses as prime and boost for LAV-IV vaccination. Of the 23 vaccinated rats challenged with 10⁵ VGE of RHV-rn1 via the intravenous route, 17 rats cleared the infection within 4 weeks. Considering that even a 10 times lower dose of RHV-rn1 produces lifelong chronic infection in all infected Lewis rats, the vaccine efficacy of LAV-IV was >75%. In our earlier studies using Adenovirus (AdV) vectors expressing the RHV nonstructural proteins for vaccination, the vaccine efficacy ranged between 50–75%, although fewer rats were used for the experimental challenge^{12,14,17}. Thus, considering the smaller group sizes, the efficacy of LAV-IV is not statistically higher than the AdV vaccine. Interestingly, in AdV-vaccinated rats, vaccine failure was associated with the emergence of T cell escape mutations in both inbred and outbred rats. The sequence analysis of the viruses in LAV-IV vaccinated rats that failed the vaccine also revealed several mutations

(Fig. 4J). However, these mutations were not located in the known T cell epitopes but rather in the E1 and NS5A proteins, indicating that CD8 T cell escape was not the primary cause of vaccine failure. Moreover, two of the six rats that developed chronic infection had very low frequencies of vaccine-primed T cells and exhibited poor expansion of antigen-specific T cells after the challenge (Fig. 4G). These observations suggest that the poor immunogenicity of LAV-IV in some rats plausibly contributed to the vaccine failure. Although the observed exhaustion of CD8 T cell antiviral function in chronic rats was expected, it further indicated that the T cell epitopes remained unchanged during the persistent viremia. Another interesting observation was that the female rats developed significantly lower titers of LAV-IV viremia after the prime dose, and this is expected since the female mice also more rapidly cleared the wild-type RHV-rn1 infection compared to male mice, and the rate of spontaneous clearance of HCV infections is reported to be significantly higher compared to males⁵⁰. However, only 3 of 5 rats that failed the LAV-IV vaccine were females. Thus, follow-up studies using larger groups of animals and analyses that consider sex as a variable are necessary.

The R3-UpA^{high} virus escaped clearance in one of the 24 vaccinated rats (Fig. 4). We anticipated that the *in vivo* rescue of high-titer stock for vaccination from RNA in a CD4-depleted rat could have facilitated the reversion of UpA mutations. However, the complete genome sequencing of the R3-UpA virus in rat-726 on day 14 indicated the absence of reversion of the introduced UpA sites (Fig. 4J). Thus, it is likely that this rat has some natural immunological deficiency, making it more susceptible to virus infection, which is not uncommon among inbred lab animals. However, persistent infection of the R3-UpA^{high} virus in rat-726 required the reversion of several introduced UpA mutations and the simultaneous emergence of novel mutations that disrupted the natural UpA sites (Fig. 4J). These observations indicate that the RHV with higher UpA remained under host selective pressure to revert UpA sites, thereby gaining replicative fitness. Finally, we used the terminal serum rat-726 to infect three naive rats, and all three rats developed chronic viremia. Thus, as reported for other virus vaccines, the use of LAV is associated with an inherent risk of reversion of attenuation⁵¹. However, LAV reversion is more likely when the attenuation is mediated by a small number of mutations (as in the Sabin poliovirus vaccines), compared to the approaches targeting CpG/UpA bias, codon usage or codon-pair changes since the attenuation originates from the effect of hundreds of mutations that are under much weaker selective pressure to revert to wild-type. It is also important to emphasize that the rat MHC and other aspects of immune variation in inbred rats are poorly documented, and the rat in question may have been genetically aberrant or immunodeficient. Finally, considering that only synonymous mutations are required to generate UpA LAV, the rare infection caused by the LAV mutant could be cured using highly effective anti-HCV therapy. Most importantly, although the nature of immunity that can protect against chronic HCV infection in humans remains poorly understood, several studies have reported that the natural clearance of HCV in humans substantially increases protection against secondary infections^{52,53}. Compared to any mRNA or protein vaccine, the LAV vaccination more closely resembles the clearance of natural HCV infection; therefore, LAV vaccination is likely to provide adequate protection against chronic infection. However, this is the first study of its kind, and further work using genetically diverse RHV variants and vaccination using a combination of different platforms is critical to make progress towards conceptualizing an LAV for HCV or its translational use in humans.

The LNP-vRNA vaccine-induced T-cell responses in vaccinated rats were also variable, likely reflecting differences in viremia between rats. Only 3 of the 24 vaccinated rats developed a chronic infection, and sequencing of these rats indicated a consistent absence of mutations in the known T cell epitopes, indicating that the differences in the pre-challenge immunity likely determined the infection outcomes. The

relatively lower frequencies of vaccine-induced IFN- γ -producing T cells and antigen-specific CD8 T cells targeting the E1 and NS5B epitopes further suggest that the differences in vaccine-primed T cell immunity may have determined the infection outcomes (Fig. 5E–G). Finally, we observed that the vaccinated rats that cleared the RHV-rn1 challenge developed significantly enhanced protection against a second RHV-rn1 reinfection (Fig. 5I). This is notable, as we had observed earlier in AdV-vaccinated rats that clearance of the RHV-rn1 challenge enhanced immunity against the chronic infection of the homologous virus and the CD8 escape variant¹⁷. Here, we also determined that the more efficient control of reinfection, as evident by the absence of viremia after reinfection, largely depended on the presence of memory CD8 T cells (Fig. 5J). These results indicate that antibody responses were relatively less important for protection in this model. More importantly, these observations suggest that although both LAV-IV and LAV-vRNA vaccines showed excellent efficacy (75–85% protection), this immunity can be enhanced on subsequent antigenic exposure. Since RHV-rn1 and R3-UpA^{high} encode identical proteins, the most likely reason for the observed enhanced protection was that the RHV-rn1 challenge resulted in higher viremia and, consequently, a higher expansion of T cells to control the infection, leading to the formation of more or better self-sustaining T_{RM} cells. Notably, our data showed that the second infection of R3-UpA^{high} virus barely produced any viremia and did not expand the memory T cell responses (Figs. 4C and 5E). These results suggest that the LAV-IV or vRNA-LNP vaccine-induced immunity and protection can be significantly enhanced by using a different vaccine platform, allowing exposure to higher amounts of antigen, such as AdV or mRNA coding homologous and heterologous proteins.

It is essential to comprehend the significance of this and previous work on the RHV rat model, particularly in light of the failure of the T cell vaccine trial in humans. In two earlier studies, conducted in inbred and outbred rat strains, we showed that recombinant adenoviral vectors encoding the RHV NS3-5B proteins reduce the incidence of persistent infection after homologous challenge^{12,14}. Prolonged or persistent RHV infection after antibody-mediated depletion of CD8 or CD4 T cells in vaccinated rats, respectively, established a critical role for cellular immunity in vaccine protection¹². Recently, a study conducted in China also demonstrated that an adenovirus-vectored vaccine can protect rats against chronic RHV infection⁵⁴. Thus, it was intriguing that the HCV vaccine regimen, despite inducing HCV-specific T-cell responses, did not prevent chronic HCV infection⁷. Considering that HCV vaccines could fail due to the vast genetic diversity of HCV and a failure to induce protective responses against non-vaccine subtypes or genotypes, we pursued our studies further to define the breadth of the adenovirus vaccine against genetically diverse RHV variants in the rat model. Notably, in a follow-up study¹⁷, we determined that the protection conferred by the adenovirus vaccine was significantly reduced against a virus with <0.5% amino acid mismatch over the polyprotein or a few CD8 T cell escape mutations. Notably, the T cell vaccine used in the human trial used NS3-5B proteins of HCV genotype 1b BK strain, but the vaccinated individuals were exposed to genetically diverse HCV variants (genotype 1a, 1b, 2b, 3a, and unknown). Of the 35 vaccinated subjects, only one individual became infected with the genotype 1b virus. The polyprotein of HCV variants, even variants of the same subtype, such as 1b, can vary by ~5% in amino acids, encompassing about 150 amino acid sites throughout the polyprotein. Furthermore, since most of these subjects were infected with different subtypes and genotypes, we expect that the protein antigen used in the vaccine differed significantly from the infecting viruses by more than 5–10%. Even then, the geometric mean peak HCV RNA level was substantially (>1 log) lower in the vaccine group than in the placebo group (152.51×10^3 IU per milliliter [95% CI, 33.5×10^3 to 686×10^3] vs. 1804.93×10^3 IU per milliliter [95% CI, 565×10^3 to 5764×10^3]), indicating vaccine-induced T cells exerted partial

control on viremia of genetically highly diverse HCV variants. Since, the adenovirus-vectored vaccine was highly sensitive to antigenic variation between vaccine and challenge viruses; for example, immunization of rats conferred 50–70% protection against a 100% identical virus but failed to protect 75% of rats against a virus with just 10–12 amino acid mutations (<0.5% amino acids)^{12,17}, the RHV studies in the rat model are not only relevant to human HCV vaccine efficacy studies but also bode well for using this model to determine the reasons for the failure of the HCV vaccine. Human studies have inherent limitations, and they are unlikely to yield a definitive or mechanistic understanding of why the vaccine failed and how a better vaccine can be designed. Thus, we believe that the RHV-rat model, because of its tractability and availability of genetically diverse RHV variants, becomes extremely useful to determine the immune correlates of protection against HCV-like chronic infection, especially since some vaccinated rats fail to clear even a homologous virus, and most vaccinated rats fail to clear a heterologous virus. It is also highly relevant that we determined earlier and in this work that the immunity induced by the adenovirus-vectored and LAV vaccines can be enhanced to protect against chronic infections of heterologous (CD8 T cell escape variant) and homologous viruses (Fig. 5I, J)¹⁷.

In conclusion, despite the availability of highly effective direct-acting antiviral therapy, approximately 1 million new HCV infections were reported in 2024⁵⁵. The development of an effective vaccine is crucial to halt the ongoing transmission of the virus, particularly in high-risk populations. Our earlier work and this study showed that the RHV rat model is valuable for defining the nature of immunity and identifying the immune correlates of protection against chronic HCV-like infection^{12,17}. Overall, our results demonstrated how to design an LAV vaccine for HCV, showing that LAV vaccination can protect against chronic infection and that LAV-induced immunity can be further enhanced by successive immunization. Thus, these results bode well for further studies using different vaccination platforms, adjuvants, and antigen combinations to enhance the LAV-induced immunity against homologous and, subsequently, against genetically diverse HCV variants.

Methods

Ethics statement

All biohazard and animal experiments were conducted in accordance with approved protocols from the Nationwide Children's Research Institute Institutional Biosafety Committee (IBS00000285) and the Institutional Animal Care and Use Committee (AR15-00116), respectively. Male and female Lewis rats were obtained from Charles Rivers Laboratories. Animals were 7–8 weeks of age at the time of study initiation.

Virus stock and quantification

We used an RHV-rn1 infectious clone-derived RNA to generate a viral inoculum in Lewis rats^{12,13,17,41}. For serum infections, rats were challenged intravenously with 10⁵ virus genomic equivalents (VGE) of clone-derived RHV-rn1 diluted in 150–200 μ L PBS by tail vein injection. RHV titers were determined as described earlier, with the only modification being that serum viral RNA was extracted using the Quick-RNA viral kit (ZYMO Research)^{12,13}. In brief, viral cDNA was generated from serum-extracted RNA using the GoScript reverse transcription kit (Promega) with random hexamer priming, followed by quantification on a StepOnePlus RT-PCR system (Applied Biosystems) using the TaqMan 2x PCR master mix (Applied Biosystems). A standard curve was generated using a linearized plasmid encoding the RHV NS3 protein, and PCR assays were done as described earlier⁴¹.

Design and synthesis of RHV mutants and LNP vaccine

The RHV-rn1 prototype sequence was mutated using SSE sequence editor⁵⁶. The boundaries of regions R2, R3 and R4 were originally

selected based on their proximity to unique restriction sites in the pUC57-RHV-rn1 clone and spanned positions 1290–2498 (length 1209 bases), 2499–3860 (1362 bases) and 3870–4781 (912 bases). Sequences were mutated using three algorithms: **CDLR**: sequences were randomized to preserve amino acid structure and dinucleotide frequencies, using the CDLR (C = Codon, D = Dinucleotide, L = Like amino acids, R = Randomize) algorithm, which maximizes the degree of sequence scrambling while maintaining coding, and native mononucleotide and dinucleotide frequencies through substitutions between equivalently coding triplets in the same upstream and downstream dinucleotide contexts. A total of 17–20 replicates were generated, and folding energies were calculated as previously described³⁹. Sequences in R2, R3, and R4 with folding energies closest to that of a mean of 49 sequences scrambled by NDR (mean folding energy difference; MFED) were selected (Table S1; Supplementary Information). **UpAH**: Frequencies of the UpA dinucleotides were maximized in the sequence while preserving coding and keeping frequencies of each mononucleotide and of CpG constant. **CpGH**: Frequencies of the CpG dinucleotide were maximized in the sequence while preserving coding and keeping frequencies of each mononucleotide and of UpA constant. Nucleotide sequences of region 2, 3, and 4 CDLR, UpAH, and CpGH mutants are provided in Supplementary Information S3.

The LNP-vRNA was made using in vitro transcribed RNA from clones and GenVoy-ILM™ reagents mixed in the Precision NanoSystems Ignite platform. The amount of LNP-encapsulated RNA was calculated using Triton-X 100 and Ribogreen binding assay, as described for Quant-it™ RiboGreen kit (ThermoFisher cat. No. R11490).

Peptides

All peptides were obtained from Genemed Synthesis as a lyophilized powder. 10 mg/mL stock solutions were prepared in a 10% DMSO-water solution and stored at –80 °C until use. The final concentration of each peptide in all functional assays was 2 or 10 μ g/mL, unless otherwise specified. For assaying T cell responses, either 18-amino-acid-long peptides overlapping by 11 amino acids and covering different proteins, or peptides representing previously identified RHV T cell epitopes in rat and mouse, were used, as described earlier^{12,16,17,41}.

Leukocyte isolation, culture, and cryopreservation

Isolation and culture of liver-infiltrating leukocytes were performed as described earlier^{12,17}. Briefly, PBS-perfused livers were minced and digested with collagenase IV solution (0.01% collagenase IV in HBSS supplemented with 40 mM HEPES) for 30 min at 37 °C. The cell suspension was gently homogenized through a stainless-steel mesh in HBSS supplemented with 10% FBS (Gibco). Cells were then isolated via 37% Percoll (GE Life Sciences) gradient density centrifugation at 500 g for 20 min followed by lysis of residual RBCs in ACK buffer (Gibco). For cytokine stimulation assays described below, cells were cultured in RPMI-1640 containing GlutaMAX and HEPES (Gibco), 10% FBS (Gibco), 50 U/mL penicillin-streptomycin (Gibco), and 55 μ M 2-mercaptoethanol (Gibco) at 37 °C. For storage, cells were cryopreserved in FBS containing 10% DMSO via standard protocol.

IFN- γ ELISpot assay

Virus-specific T cells were enumerated with the anti-mouse IFN- γ enzyme-linked immunosorbent (ELISPOT) assay (U-Cytech) according to the manufacturer's protocol. Cells were cultured at 2×10^5 cells per well in duplicate and stimulated with peptides, or media alone or Concanavalin-A (Sigma; 5 μ g/mL) as negative and positive controls, respectively, for 40–48 h prior to plate development. The total number of spot-forming cells (SFCs) was calculated by subtracting the mean number of spots in the negative wells from the mean number of spots in test wells, followed by normalization to 106 cells. A positive response was defined as >3 times the response of background wells and >50 SFCs/106 cells after normalization.

Quantification of intracellular cytokine production

For detection of RHV-specific intracellular cytokine production, one million cells were stimulated in 96-well round-bottom plates with peptide(s) representing CD8 and CD4 T cell epitopes^{12,16,17}, or media alone or PMA/Ionomycin (BioLegend) as negative and positive controls, respectively, for 5-h in the presence of GolgiPlug (BD Biosciences). Following incubation, cells were surface stained for CD3, CD4, and CD8 (20 min), fixed and permeabilized using the cytofix/cytoperm kit (BD Biosciences), and intracellularly stained for IFN- γ , TNF- α , and IL-2 (60 min at 4 °C). Dead cells were removed using the LIVE/DEAD Fixable Near-IR Dead Cell Stain kit (Invitrogen). A positive response was defined as >3 times the background staining of the negative control sample. The percentage of cytokine-positive cells was then calculated by subtracting the frequency of positive events in negative control samples from that of test samples.

Tetramer staining

MHC class I RT1-Aⁱ tetramers for the Lewis rat were obtained from the NIH Tetramer Core Facility. Tetramers were assessed against intrahepatic lymphocytes from immunized rats^{12,17}. Samples from naïve animals were used as a negative control. Cells were stained with class I tetramers for 60 min at 4 °C. After washing, cells were stained with LIVE/DEAD Fixable Near-IR Dead Cell Stain kit and surface/intracellular markers as described above. For staining of mouse T cells, biotinylated MHC class I H2-D^b and class II I-A^b monomers specific for the RHV NS₉₆₈ and NS₁₂₆₅ epitopes were obtained from the NIH Tetramer Core Facility and tetramerized with streptavidin-PE (Prozyme)⁴¹. For direct visualization of virus-specific T cell populations, liver-infiltrating leukocytes or splenocytes were stained for 60 min at 4 °C (1:500) for Class-I and 90 min at 37 °C for Class-II tetramer, followed by labeling with antibodies for surface markers. Subsequently, cells were stained LIVE/DEAD Fixable Near-IR Dead Cell Stain kit, fixed, and permeabilized by transcription factor buffer set (eBiosciences) before staining for transcription factors.

In vivo cell depletions

To deplete CD8 T cells in vivo, vaccinated rats were injected intravenously with 0.5 mg anti-rat CD8 α depleting (OX-8) or IgG1 isotype control antibodies (BioXcell) 3 days before virus infection. Rats received two additional doses of 0.5 mg on days 7 and 14 post-infection to prolong depletion. For CD4⁺ cell depletions, vaccinated rats received 1.0 mg anti-rat CD4 depleting (OX38) or IgG2a isotype control antibodies (BioXcell) on days -3, 7, and 14 of infection. Depletion and recovery of cells in blood were tracked via flow cytometry using the G28 and OX-35 antibodies, which bind separate CD8 and CD4 epitopes than the OX-8 and OX-38 clones, respectively. In brief, heparinized blood was stained for 20 min with anti-rat CD3 and CD8 or CD4 antibodies, followed by direct RBC lysis and fixation (BD lyse/fix buffer).

Flow cytometry data analysis and visualization

The details of the antibodies used to analyze rat and mouse immune cells are provided in Table S2. Flow cytometry data were analyzed using FlowJo software v.10.8.1. Protein expression levels were extracted as percentages and/or as MFI numerical values.

Statistical analysis

Data are presented as either individual values or the mean \pm SEM or replicate or groups of animals. To compare values obtained from two or more groups, Student's *t*-test or one-way ANOVA was performed. All statistical analyses were done in GraphPad PRISM 10.3.1. Only *p*-values <0.01 or 0.05 were considered statistically significant and are shown as <0.05 (*), <0.01 (**), <0.001 (***), and <0.0001 (****).

Reporting summary

Further information on research design is available in the Nature Portfolio Reporting Summary linked to this article.

Data availability

Sequence data shown in Fig. 4J was submitted to GenBank under accession numbers PV639513-PV639519. Raw data associated with Figs. 1A, D, E, 2A, B, E, F, 3A, C, F, G, 4A, C, G, 5C, J are provided in Supplementary Information and Source Data file. Source data are provided with this paper.

References

- Houghton, M. The long and winding road leading to the identification of the hepatitis C virus. *J. Hepatol.* **51**, 939–948 (2009).
- Ghany, M. G. et al. The 2020 Nobel Prize for medicine or physiology for the discovery of Hepatitis C Virus: A triumph of curiosity and persistence. *Hepatology* **74**, 2813–2823 (2021).
- Liang, T. J., Feld, J. J., Cox, A. L. & Rice, C. M. Controlled human infection model - fast track to HCV Vaccine?. *N. Engl. J. Med.* **385**, 1235–1240 (2021).
- Hartlage, A. S. & Kapoor, A. Hepatitis C Virus vaccine research: time to put up or shut up. *Viruses* **13**, <https://doi.org/10.3390/v13081596> (2021).
- Bailey, J. R., Barnes, E. & Cox, A. L. Approaches, progress, and challenges to Hepatitis C vaccine development. *Gastroenterology* **156**, 418–430 (2019).
- Bartenschlager, R. et al. Critical challenges and emerging opportunities in hepatitis C virus research in an era of potent antiviral therapy: Considerations for scientists and funding agencies. *Virus Res.* **248**, 53–62 (2018).
- Page, K. et al. Randomized trial of a vaccine regimen to prevent chronic HCV infection. *N. Engl. J. Med.* **384**, 541–549 (2021).
- Smith, D. B. et al. Expanded classification of hepatitis C virus into 7 genotypes and 67 subtypes: updated criteria and genotype assignment web resource. *Hepatology* **59**, 318–327 (2014).
- Tonnerre, P. et al. Differentiation of exhausted CD8(+) T cells after termination of chronic antigen stimulation stops short of achieving functional T cell memory. *Nat. Immunol.* **22**, 1030–1041 (2021).
- Messina, J. P. et al. Global distribution and prevalence of hepatitis C virus genotypes. *Hepatology* **61**, 77–87 (2015).
- Firth, C. et al. Detection of zoonotic pathogens and characterization of novel viruses carried by commensal *Rattus norvegicus* in New York City. *mBio* **5**, e01933–01914 (2014).
- Hartlage, A. S. et al. Vaccination to prevent T cell subversion can protect against persistent hepacivirus infection. *Nat. Commun.* **10**, 1113 (2019).
- Trivedi, S. et al. Viral persistence, liver disease and host response in Hepatitis C-like virus rat model. *Hepatology*, <https://doi.org/10.1002/hep.29494> (2017).
- Atcheson, E. et al. Use of an outbred rat hepacivirus challenge model for design and evaluation of efficacy of different immunization strategies for Hepatitis C Virus. *Hepatology*, <https://doi.org/10.1002/hep.30894> (2019).
- Wolfisberg, R. et al. Replicons of a rodent Hepatitis C model virus permit selection of highly permissive cells. *J. Virol.* **93**, e00733–19 (2019).
- Hartlage, A. S., Walker, C. M. & Kapoor, A. Priming of antiviral CD8 T cells without effector function by a persistently replicating Hepatitis C-like virus. *J. Virol.* **94**, <https://doi.org/10.1128/JVI.00035-20> (2020).
- Hartlage, A. S., Dravid, P., Walker, C. M. & Kapoor, A. Adenovirus-vectored T cell vaccine for hepacivirus shows reduced effectiveness against a CD8 T cell escape variant in rats. *PLoS Pathog.* **17**, e1009391 (2021).
- Grakoui, A. et al. HCV persistence and immune evasion in the absence of memory T cell help. *Science* **302**, 659–662 (2003).
- Bowen, D. G. & Walker, C. M. Adaptive immune responses in acute and chronic hepatitis C virus infection. *Nature* **436**, 946–952 (2005).

20. Timme, R. et al. Viral and immunological determinants of hepatitis C virus clearance, persistence, and disease. *Proc. Natl. Acad. Sci. USA* **99**, 15661–15668 (2002).
21. Wolski, D. et al. Early Transcriptional divergence marks virus-specific primary human CD8(+) T Cells In Chronic Versus Acute Infection. *Immunity* **47**, 648–663.e648 (2017).
22. Schulze Zur Wiesch, J. et al. Broadly directed virus-specific CD4+ T cell responses are primed during acute hepatitis C infection, but rapidly disappear from human blood with viral persistence. *J. Exp. Med.* **209**, 61–75 (2012).
23. Billerbeck, E. et al. Mouse models of acute and chronic hepatitis C virus infection. *Science* **357**, 204–208 (2017).
24. Hartlage, A. S., Walker, C. M. & Kapoor, A. Priming of antiviral CD8 T cells without effector function by a persistently replicating hepatitis C-like virus. *J. Virol.*, <https://doi.org/10.1128/JVI.00035-20> (2020).
25. Burns, C. C. et al. Modulation of poliovirus replicative fitness in HeLa cells by deoptimization of synonymous codon usage in the capsid region. *J. Virol.* **80**, 3259–3272 (2006).
26. Nogales, A. et al. Influenza A virus attenuation by codon deoptimization of the NS gene for vaccine development. *J. Virol.* **88**, 10525–10540 (2014).
27. Meng, J., Lee, S., Hotard, A. L. & Moore, M. L. Refining the balance of attenuation and immunogenicity of respiratory syncytial virus by targeted codon deoptimization of virulence genes. *mBio* **5**, e01704–e01714 (2014).
28. Coleman, J. R. et al. Virus attenuation by genome-scale changes in codon pair bias. *Science* **320**, 1784–1787 (2008).
29. Mueller, S., Papamichail, D., Coleman, J. R., Skiena, S. & Wimmer, E. Reduction of the rate of poliovirus protein synthesis through large-scale codon deoptimization causes attenuation of viral virulence by lowering specific infectivity. *J. Virol.* **80**, 9687–9696 (2006).
30. Mueller, S. et al. Live attenuated influenza virus vaccines by computer-aided rational design. *Nat. Biotechnol.* **28**, 723–726 (2010).
31. Le Nouen, C. et al. Attenuation of human respiratory syncytial virus by genome-scale codon-pair deoptimization. *Proc. Natl. Acad. Sci. USA* **111**, 13169–13174 (2014).
32. Fros, J. J. et al. The dinucleotide composition of the Zika virus genome is shaped by conflicting evolutionary pressures in mammalian hosts and mosquito vectors. *PLoS Biol.* **19**, e3001201 (2021).
33. Fros, J. J. et al. CpG and UpA dinucleotides in both coding and non-coding regions of echovirus 7 inhibit replication initiation post-entry. *eLife* **6**, <https://doi.org/10.7554/eLife.29112> (2017).
34. Gaunt, E. et al. Elevation of CpG frequencies in influenza A genome attenuates pathogenicity but enhances host response to infection. *eLife* **5**, e12735 (2016).
35. Tulloch, F., Atkinson, N. J., Evans, D. J., Ryan, M. D. & Simmonds, P. RNA virus attenuation by codon pair deoptimisation is an artefact of increases in CpG/UpA dinucleotide frequencies. *eLife* **3**, e04531 (2014).
36. Goonawardane, N., Nguyen, D. & Simmonds, P. Association of Zinc finger antiviral protein binding to viral genomic RNA with attenuation of replication of Echovirus 7. *mSphere* **6**, <https://doi.org/10.1128/mSphere.01138-20> (2021).
37. Odon, V. et al. The role of ZAP and OAS3/RNaseL pathways in the attenuation of an RNA virus with elevated frequencies of CpG and UpA dinucleotides. *Nucleic Acids Res.* **47**, 8061–8083 (2019).
38. Ploss, A. & Kapoor, A. Animal Models of Hepatitis C Virus Infection. *Cold Spring Harb Perspect. Med.* **10**, <https://doi.org/10.1101/cshperspect.a036970> (2020).
39. Simmonds, P., Tuplin, A. & Evans, D. J. Detection of genome-scale ordered RNA structure (GORS) in genomes of positive-stranded RNA viruses: Implications for virus evolution and host persistence. *RNA* **10**, 1337–1351 (2004).
40. Goncalves-Carneiro, D. & Bieniasz, P. D. Mechanisms of Attenuation by Genetic Recoding of Viruses. *mBio* **12**, <https://doi.org/10.1128/mBio.02238-20> (2021).
41. Dravid, P. et al. Phenotype and fate of liver-resident CD8 T cells during acute and chronic hepatitis C virus infection. *PLoS Pathog.* **19**, e1011697 (2023).
42. Walker, C. M. Adaptive immunity to the hepatitis C virus. *Adv. Virus Res.* **78**, 43–86 (2010).
43. Wolfisberg, R. et al. Neutralization and receptor use of infectious culture-derived rat hepatitis C virus as a model for HCV. *Hepatology* **76**, 1506–1519 (2022).
44. Wolfisberg, R. et al. Molecular determinants of mouse adaptation of Rat Hepacivirus. *J. Virol.* **97**, e0181222 (2023).
45. Brown, A. J. et al. Host genetic variation guides hepatitis C virus clearance, chronicity, and liver fibrosis in mice. *Hepatology* **79**, 183–197 (2024).
46. Stoppeler, S. et al. Gender and strain-specific differences in the development of steatosis in rats. *Lab. Anim.* **47**, 43–52 (2013).
47. Simmonds, P. et al. Impact of virus subtype and host IFNL4 genotype on large-scale RNA structure formation in the genome of hepatitis C virus. *RNA* **26**, 1541–1556 (2020).
48. McNamara, H. A. et al. Up-regulation of LFA-1 allows liver-resident memory T cells to patrol and remain in the hepatic sinusoids. *Sci. Immunol.* **2**, <https://doi.org/10.1126/sciimmunol.aaj1996> (2017).
49. Loyal, L. et al. SLAMF7 and IL-6R define distinct cytotoxic versus helper memory CD8(+) T cells. *Nat. Commun.* **11**, 6357 (2020).
50. Bakr, I. et al. Higher clearance of hepatitis C virus infection in females compared with males. *Gut* **55**, 1183–1187 (2006).
51. Lauring, A. S., Jones, J. O. & Andino, R. Rationalizing the development of live attenuated virus vaccines. *Nat. Biotechnol.* **28**, 573–579 (2010).
52. Osburn, W. O. et al. Spontaneous control of primary hepatitis C virus infection and immunity against persistent reinfection. *Gastroenterology* **138**, 315–324 (2010).
53. Sacks-Davis, R. et al. Hepatitis C virus reinfection and spontaneous clearance of reinfection—the InC3 Study. *J. Infect. Dis.* **212**, 1407–1419 (2015).
54. Luo, S. et al. Protection of Novel Adenovirus vectored vaccine in rats against wild-type hepatitis C virus and variant infections. *Liver Int* **45**, e70045 (2025).
55. WHO Hepatitis and STIs Programmes (HHS) Global HIV 1–242 (2024).
56. Simmonds, P. SSE: a nucleotide and amino acid sequence analysis platform. *BMC Res Notes* **5**, 50, (2012).

Acknowledgements

We thank the NIH Tetramer Core Facility for constructing the tetramers used in this study. This study was supported by NIH awards AI171928, AI151175, AI185926, and AI183877, and in part by the intramural research program of the National Institute of Dental and Craniofacial Research. The funders had no role in the study design, data collection and analysis, the decision to publish, or the preparation of the manuscript.

Author contributions

S.T. and P.D. performed experiments, analyzed data, and wrote the manuscript. S.M., K.S.K., N.R., J.K., R.C., C.C. and H.S. performed experiments, analyzed, and reviewed data. T.C.P., P.D.B. and A.G. reviewed data and provided scientific support. H.S., P.S. and A.K. analyzed data, conceived and oversaw the study, provided scientific and financial support, and wrote the manuscript.

Competing interests

The authors declare no competing interests.

Additional information

Supplementary information The online version contains supplementary material available at <https://doi.org/10.1038/s41467-025-62813-8>.

Correspondence and requests for materials should be addressed to Amit Kapoor.

Peer review information *Nature Communications* thanks the anonymous reviewers for their contribution to the peer review of this work. A peer review file is available.

Reprints and permissions information is available at <http://www.nature.com/reprints>

Publisher's note Springer Nature remains neutral with regard to jurisdictional claims in published maps and institutional affiliations.

Open Access This article is licensed under a Creative Commons Attribution-NonCommercial-NoDerivatives 4.0 International License, which permits any non-commercial use, sharing, distribution and reproduction in any medium or format, as long as you give appropriate credit to the original author(s) and the source, provide a link to the Creative Commons licence, and indicate if you modified the licensed material. You do not have permission under this licence to share adapted material derived from this article or parts of it. The images or other third party material in this article are included in the article's Creative Commons licence, unless indicated otherwise in a credit line to the material. If material is not included in the article's Creative Commons licence and your intended use is not permitted by statutory regulation or exceeds the permitted use, you will need to obtain permission directly from the copyright holder. To view a copy of this licence, visit <http://creativecommons.org/licenses/by-nc-nd/4.0/>.

© The Author(s) 2025